Monthly Notices
of the
ROYAL ASTRONOMICAL SOCIETY

MNRAS **495,** L7–L11 (2020)
Advance Access publication 2020 March 19

doi:10.1093/mnrasl/slaa048

A new proxy to estimate the cosmic ray ionization rate in dense cores

S. Bovino,[1]★ S. Ferrada-Chamorro,[1] A. Lupi,[2] D. R. G. Schleicher[1] and P. Caselli[3]

[1]*Departamento de Astronomía, Facultad Ciencias Físicas y Matemáticas, Universidad de Concepción, Av. Esteban Iturra s/n Barrio Universitario, Casilla 160, Concepción, Chile*
[2]*Scuola Normale Superiore, Piazza dei Cavalieri 7, I-56126 Pisa, Italy*
[3]*Centre for Astrochemical Studies, Max-Planck-Institute for Extraterrestrial Physics, Giessenbachstrasse 1, D-85748 Garching, Germany*

Accepted 2020 March 11. Received 2020 March 11; in original form 2020 February 17

ABSTRACT

Cosmic rays are a global source of ionization, and the ionization fraction represents a fundamental parameter in the interstellar medium. Ions couple to magnetic fields, and affect the chemistry and the dynamics of star-forming regions as well as planetary atmospheres. However, the cosmic ray ionization rate represents one of the bottlenecks for astrochemical models, and its determination is one of the most puzzling problems in astrophysics. While for diffuse clouds reasonable values have been provided from H_3^+ observations, for dense clouds, due to the lack of rotational transitions, this is not possible, and estimates are strongly biased by the employed model. We present here an analytical expression, obtained from first principles, to estimate the cosmic ray ionization rate from observational quantities. The theoretical predictions are validated with high-resolution 3D numerical simulations and applied to the well-known core L1544; we obtained an estimate of $\zeta_2 \sim 2$–3×10^{-17} s^{-1}. Our results and the analytical formulae provided represent the first model-independent robust tool to probe the cosmic ray ionization rate in the densest part of star-forming regions (on spatial scales of $R \leq 0.05$ pc). An error analysis is presented to give statistical relevance to our study.

Key words: astrochemistry – hydrodynamics – methods: numerical – cosmic rays.

1 INTRODUCTION

The densest regions of molecular clouds where star formation is beginning are characterized by a high degree of CO depletion (e.g. Caselli et al. 1999; Fontani et al. 2012; Giannetti et al. 2014; Sabatini et al. 2019) and high levels of deuteration (e.g. Ceccarelli et al. 2014). In particular, the deuterated forms of the main ion H_3^+ (e.g. H_2D^+) dominate the chemistry during the early stages prior to the formation of a protostellar object (Pagani, Salez & Wannier 1992; Caselli et al. 2003; Giannetti et al. 2019).

The formation of H_3^+ and more generally the ion-neutral chemistry characterizing these regions are driven by cosmic rays (CRs), i.e. highly energetic particles that can penetrate the dense regions within molecular clouds starting a chain of reactions that leads to the formation of key tracers (e.g. HCO^+, N_2H^+). H_3^+ is indeed considered a key molecule to determine the CR ionization rate (CRIR), in particular due to the simple chain of reactions involved in its chemistry. Each ionization of H_2 through CRs leads to the formation of H_3^+, which is mainly destroyed by neutrals (e.g. CO and O; Dalgarno 2006).

CRs have a strong effect on the deuteration process itself, this being affected by H_3^+, the ion that starts the deuteration process by forming H_2D^+. Many authors have shown, through simple (e.g. Caselli et al. 2008; Kong et al. 2015) or complex theoretical models (Körtgen et al. 2018; Bovino et al. 2019), that a higher CRIR favours the deuteration process, in particular shortening the time to reach typical observed values. Determining the time-scale for deuteration is of fundamental importance when the deuterium fractionation is used as a chemical clock of star-forming regions (see e.g. Fontani et al. 2011; Brünken et al. 2014), and providing an estimate for the CRIR has then a crucial effect on our interpretation of the physics of star formation (e.g. ambipolar diffusion, time-scales, chemistry).

The CRIR has been probed through a mix of observations and chemical models in diffuse clouds starting from the pioneering work of Black, Hartquist & Dalgarno (1978) based on OH and HD observations. Quantitative measurements were then provided through observations of H_3^+ in absorption in diffuse and dense clouds by Indriolo (2012), Neufeld & Wolfire (2017), Geballe & Oka (1996), and McCall et al. (1999). Additional work was pursued by van der Tak & van Dishoeck (2000), with a different approach based on $H^{13}CO^+$ in dense clouds towards massive young stars. Overall, in particular for dense clouds, estimates of the ionization rate of hydrogen atom ζ_H are in the range $\sim 3 \times 10^{-17}$ to 10^{-16} s^{-1}. From now on, we will consider $\zeta_2 = 2.3\zeta_H$ as the CRIR of hydrogen molecule.

Analytical approaches, based on simple steady-state assumptions, have been explored in different works by Caselli et al.

★ E-mail: stefanobovino@astro-udec.cl

(1998), Caselli (2002), Ceccarelli et al. (2004), and Vaupré et al. (2014). These works were focused on the estimate of the ionization fraction first and then CRIR from DCO^+, HCO^+, and CO. However, Shingledecker et al. (2016) have shown that estimates based on the ratio $[HCO^+]/[DCO^+]$ strongly depend on the initial H_2 *ortho*-to-*para* ratio and other dynamical quantities like the age of the source, the temperature, and the density.

A pure theoretical method based on dust temperature evaluation has been proposed and applied to L1544 by Ivlev et al. (2019). The latter provided an upper limit of the CRIR of $\zeta_2 \sim 10^{-16}$ s^{-1}. Recently, a new method has been proposed by Bialy (2020), who suggested to observe line emission of H_2 rovibrational transitions to estimate the CRIR. Overall, there is no consensus on the final value of ζ_2 in dense regions and estimates vary by orders of magnitude.

In this letter, we aim at providing a robust tool to estimate the CRIR in dense cores from first principles. Our approach is validated by high-resolution numerical simulations and tested under different dynamical and chemical conditions. In the following sections, we shall briefly present the simulations, the methodology, and the error estimates. We then discuss some of the caveats and the applicability of the presented method.

2 H_3^+ FROM ITS DEUTERATED FORMS AND CRIR

Under the steady-state assumption, Caselli (2002) provided useful formulae that can be employed to estimate, for instance, the ionization fraction of dense regions. Starting from their equations (9) and (10) and the work by McCall et al. (1999), we have built a set of new correlations that can be employed to estimate the CRIR. The entire analysis is based on observable quantities, i.e. column densities. From the observations of H_2D^+ and other H_3^+ isotopologues (enhanced in the cold and dense regions of molecular clouds), we can obtain an estimate of the H_3^+ column density:

$$N[H_3^+] = \frac{1}{3}\frac{D[H_3^+]}{R_D}, \tag{1}$$

where R_D is the deuterium fractionation of HCO^+,

$$R_D = \frac{N[DCO^+]}{N[HCO^+]}, \tag{2}$$

and $D[H_3^+] = N[H_2D^+] + N[D_2H^+]\gamma_1 + N[D_3^+]\gamma_2$, with $\gamma_1 = 1 - R_D$ and $\gamma_2 = 2 - R_D$, and each term represents the sum over the different isomers (*ortho*, *para*, and *meta*). We include all H_3^+ isotopologues, to account for the conversion of H_2D^+ into D_2H^+, and finally into D_3^+. These represent the additional terms compared to the original Caselli (2002) derivation, where we have considered that HCO^+ can form also from D_2H^+, and DCO^+ from D_2H^+ as well as D_3^+. Note that the correction factors are negligible if $R_D \leq 0.1$. We test different formulae that gradually include more isotopologues to provide different levels of approximations and an error estimate for the different formulae. We will refer to $D[H_3^+]$ equal to (1) only *o*-H_2D^+, (2) the total H_2D^+ (*ortho* + *para*), (3) total H_2D^+ and total D_2H^+,[1] (4) all the isotopologues (i.e. with D_3^+),[2] and (5) only the species observable with ALMA/APEX, i.e. $D[H_3^+] = o\text{-}H_2D^+ + p\text{-}D_2H^+$.

[1]To employ cases (2) and (3), SOFIA observations would be needed as the *p*-H_2D^+ and *o*-D_2H^+ transitions fall in the THz regime.

[2]Note that D_3^+ cannot be observed in high-extinction regions as it has transitions in the near-infrared, so this formula cannot be applied from an observational point of view but we report it for completeness.

Once obtained the column density of H_3^+, we can have a rough estimate of ζ_2 (see e.g. Oka 2019) by balancing formation and destruction of H_3^+ (in steady state):

$$\zeta_2 = \bar{\alpha} k_{CO}^{H_3^+} \frac{N[CO]N[H_3^+]}{N[H_2]}\frac{1}{L}, \tag{3}$$

with $k_{CO}^{H_3^+}$ the destruction rate of H_3^+ by CO, which we consider the main destruction path for H_3^+, L the path-length over which the column densities are estimated, and $\bar{\alpha}$ a correction factor that encapsulates any missing effect in the approximation. The factor is calibrated for each of the proposed approximations in the next sections. We are assuming here that the ratio between number densities is the same as the ratio between column densities, then $X_{CO} = n_{CO}/n_{H_2} = N[CO]/N[H_2]$. Other chemical reactions affecting H_3^+ destruction, like destruction via atomic oxygen (assumed to be highly depleted on to dust grains in dense regions), or dissociative recombination with electrons are neglected. The latter represents our strongest assumption but allows us to remove a dependence on the ionization fraction. However, we have also to consider that $x_e \leq 10^{-8}$ in the very central region of the cores and then our choice is not going to have a huge impact on the final results.

3 RESULTS

We use the suite of simulations of collapsing high-mass cores and clumps presented by Bovino et al. (2019), plus a new set of simulations where we change the CRIR. The simulations were performed with GIZMO (Hopkins 2015), assuming an isothermal ($T = 15$ K) Bonnor–Ebert sphere as initial condition. We account for magnetic fields, turbulence, and detailed chemistry, with C–N–O bearing species including N_2H^+, CO, HCO^+, and their deuterated forms, and time-dependent adsorption and desorption processes. The mass and spatial resolution of our simulations are 2×10^{-4} $M_\odot$ and 10^{-4} pc, respectively, and all the realizations showed fast deuterium enrichment, in particular for H_3^+ and N_2H^+, and high levels of CO depletion ($f_{dep} \sim 20$–500).

In our simulations, the CRIR is set to a constant value, and it is varied to assess how it affects the deuteration time-scale and the depletion process. We have selected a reference core of 20 $M_\odot$, with a size of 0.17 pc, supervirial ($\alpha_{vir} = 4.32$), with an average density of $\langle n \rangle = 2.2 \times 10^4$ cm^{-3}. This is what we call a 'slow collapse' core, highly supported by turbulence and magnetic fields with an average free-fall time of 260 kyr. Maps of the column densities of the main tracers are shown in Fig. 1 after 30 kyr of evolution. At this stage, the core is slowly collapsing, supported by turbulence, and it is starting to fragment. Column densities of D_2H^+ and D_3^+ are at least two orders of magnitude lower compared to H_2D^+. The deuteration fraction of HCO^+ (i.e. R_D) is on average around 10^{-3}, while CO is starting to freeze out ($f_{dep} \sim 5$), in particular in the centre of the core. These represent the quantities that we plug into equations (1)–(3) to estimate the CRIR.

In Fig. 2, we report the H_3^+ column density profile obtained from the simulation in comparison with the one obtained from our analytical formula (equation 1) on a scale of 0.05 pc for the different approximations.

As D_3^+ and D_2H^+ are not yet formed in relevant amounts, the effect of including them in $D[H_3^+]$ or not is not dramatic. The main difference between the approximations comes from the inclusion (or not) of the *para* form of H_2D^+ that at this stage is the only relevant isotopologue together with its *ortho* counterpart. Compared to the

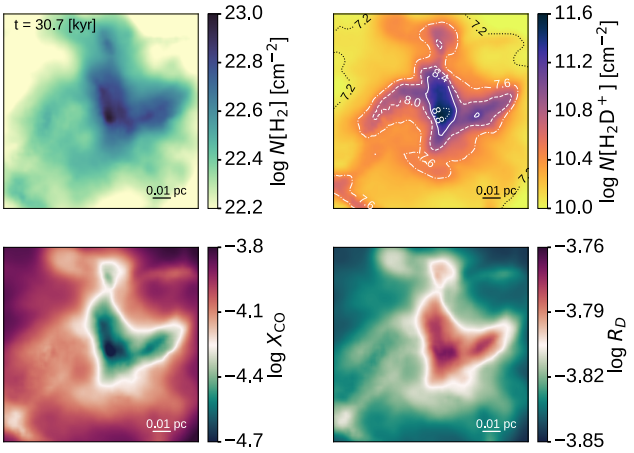

Figure 1. Total H_2 (top left), R_D (bottom right), and X_{CO} (bottom left) maps for our reference run at ∼30 kyr of evolution. H_2D^+ map is shown in the top right panel, with the overplotted white contours representing the $N(D_2H^+)$. The column densities are obtained on scales of 0.2 pc.

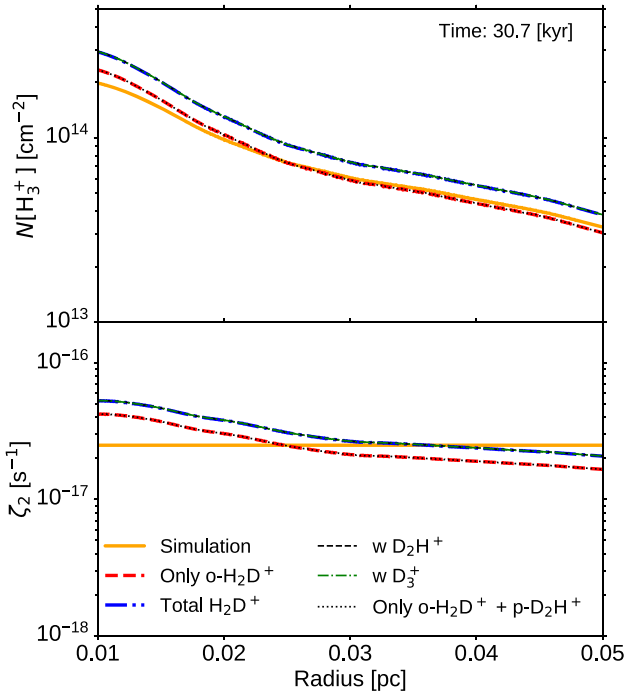

Figure 2. Radial profile of the H_3^+ column density (top panel) and CRIR (bottom panel) for different analytical approximations, compared to the values in the simulation. The results are shown after 30 kyr of evolution. We show different approximations depending on how many isotopologues have been included in equation (1).

column density obtained from simulations, we notice a very small error whatever the assumption we employ. This is also reflected in the CRIR profile (bottom panel of Fig. 2) where we are able to recover the CRIR set in the simulation with our analytical formula within a factor of less than 2 depending on the isotopologues that we include.

While the analytical formula is working very well at early dynamical times, the error increases as we proceed in time. This is highlighted in Fig. 3, where we report the H_3^+ column density

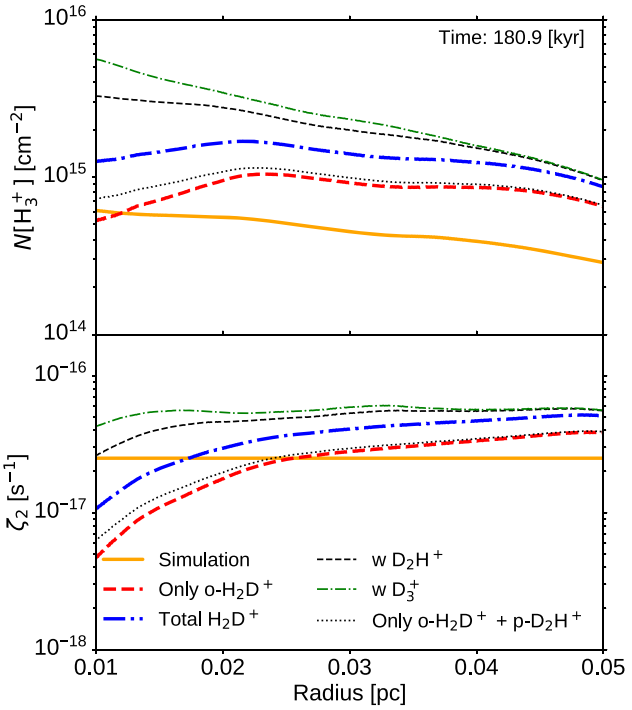

Figure 3. Same as Fig. 2, but after 180 kyr.

and the CRIR at ∼180 kyr. We see that the inferred column density is now affected by a larger error; on average, it is overestimated by a factor of 5. The overestimate is not surprising considering that we are neglecting important destruction paths for H_3^+ (e.g. O and e^-). However, when we look at the estimate of the CRIR, the final error is lower, and still depends on the formula employed and on the considered spatial scale.

3.1 Error estimates

Because of the significant variations in the CRIR estimate, both in space and in time, the best approach to get an error estimate is via a statistical analysis of the results, averaged over time and over different spatial scales. We proceed in two steps: (i) we first construct a temporal evolution of the mean CRIR estimated from the average column densities over different spatial scales θ ranging in between 0.02 and 0.05 pc, and then (ii) average each CRIR history in time to obtain a mean value and its standard deviation. Finally, we estimate a single representative CRIR for each approximation by applying a *weighted mean* to the different θ, defined as

$$\bar{\zeta}_2 = \frac{\sum_{i=1}^{N} w(\theta_i)\langle\zeta_2(\theta_i)\rangle}{\sum_{i=1}^{N} w(\theta_i)}, \quad (4)$$

where $\langle\zeta_2(\theta_i)\rangle$ is the time average on the different spatial scales. Assuming that each spatial scale gives a statistically independent measure of the CRIR, the weights can be defined as $w(\theta_i) = 1/\sigma^2(\theta_i)$, $\sigma(\theta_i)$ being the standard deviation for the ith scale. The standard error for the weighted mean is then calculated as

$$\sigma_{\bar{\zeta}_2} = \left(\sqrt{\sum_{i=1}^{N} w(\theta_i)}\right)^{-1}. \quad (5)$$

This is applied to a suite of simulations with different dynamical initial conditions and initial CRIR. Final results are reported in

Table 1. The *Method* column refers to which species are used to calculate $D[H_3^+]$ in equation (1). (1) Only *o*-H_2D^+, (2) total H_2D^+, (3) the observable isotopologues (H_2D^+ and D_2H^+), (4) all the isotopologues, i.e. we also include D_3^+, and (5) only the species observable with ALMA/APEX (*o*-H_2D^+ and *p*-D_2H^+). The last two columns report the correction factor α and its uncertainty. Details on the different simulations can be found in Bovino et al. (2019). The H_2 *ortho*-to-*para* ratio (OPR) is set to 3 unless specified.

Method	$\bar{\zeta}_2$	$\sigma_{\bar{\zeta}_2}$	α	σ_α
M0: fast collapse core, $\zeta_2 = 2.5 \times 10^{-17}$ s^{-1}				
(1)	3.3466×10^{-17}	5.7996×10^{-18}	0.7470	0.1295
(2)	6.2106×10^{-17}	1.1092×10^{-17}	0.4025	0.0719
(3)	6.2418×10^{-17}	1.1162×10^{-17}	0.4005	0.0716
(4)	6.2418×10^{-17}	1.1162×10^{-17}	0.4005	0.0716
(5)	4.9622×10^{-17}	8.8558×10^{-18}	0.5038	0.0899
M1: slow collapse core, $\zeta_2 = 2.5 \times 10^{-17}$ s^{-1}				
(1)	3.1568×10^{-17}	9.8170×10^{-18}	0.7919	0.2463
(2)	5.3419×10^{-17}	1.4347×10^{-17}	0.4680	0.1257
(3)	6.5516×10^{-17}	1.2758×10^{-17}	0.3816	0.0743
(4)	7.3836×10^{-17}	1.2076×10^{-17}	0.3386	0.0554
(5)	3.9854×10^{-17}	1.1719×10^{-17}	0.6273	0.1844
M1: slow collapse core, $\zeta_2 = 2.5 \times 10^{-18}$ s^{-1}				
(1)	3.6303×10^{-18}	6.1257×10^{-19}	0.6886	0.1162
(2)	5.6742×10^{-18}	9.4603×10^{-19}	0.4406	0.0735
(3)	5.6976×10^{-18}	9.4811×10^{-19}	0.4388	0.0730
(4)	5.6977×10^{-18}	9.4811×10^{-19}	0.4388	0.0730
(5)	4.5361×10^{-18}	7.5718×10^{-19}	0.5511	0.0920
M1: slow collapse core, $\zeta_2 = 2.5 \times 10^{-16}$ s^{-1}				
(1)	9.2224×10^{-17}	6.1415×10^{-17}	2.7110	1.8050
(2)	1.7484×10^{-16}	1.0019×10^{-16}	1.4300	0.8194
(3)	2.6436×10^{-16}	1.3270×10^{-16}	0.9457	0.4747
(4)	3.0737×10^{-16}	1.4427×10^{-16}	0.8134	0.3818
(5)	1.1621×10^{-16}	7.2152×10^{-17}	2.1510	1.3360
M1: slow collapse core, $\zeta_2 = 2.5 \times 10^{-17}$ s^{-1}, OPR(H_2) = 0.1				
(1)	2.3604×10^{-17}	8.7352×10^{-18}	1.0590	0.3920
(2)	4.3713×10^{-17}	1.3791×10^{-17}	0.5719	0.1804
(3)	6.2305×10^{-17}	1.5183×10^{-17}	0.4013	0.0978
(4)	7.3752×10^{-17}	1.4537×10^{-17}	0.3390	0.0668
(5)	3.0594×10^{-17}	1.0435×10^{-17}	0.8172	0.2787
M3: fragmented clump: $\zeta_2 = 2.5 \times 10^{-17}$ s^{-1}				
(1)	2.7583×10^{-17}	5.1299×10^{-18}	0.9064	0.1686
(2)	4.9326×10^{-17}	9.2854×10^{-18}	0.5068	0.0954
(3)	5.0298×10^{-17}	9.5295×10^{-18}	0.4970	0.0942
(4)	5.0336×10^{-17}	9.5365×10^{-18}	0.4967	0.0941
(5)	3.9064×10^{-17}	7.3345×10^{-18}	0.6400	0.1202

Table 1, where we specify the type of simulation and the employed CRIR. Our estimate of the average CRIR is very close to the real value, with changes within a factor of $\alpha = \zeta_2^{\rm real}/\bar{\zeta}_2 \sim 0.30$–$0.8$, with the only exception being the case with a very high CRIR, where the error is still within a factor of 2, but we notice an inverted trend for some of the formulae (e.g. a factor of 2.7 for the formula where we employ only *o*-H_2D^+). We calculate the standard deviation of the individual α by propagating the errors and then computing a weighted mean to obtain an average correction factor $\bar{\alpha}$ to be used in equation (3), with its corresponding uncertainty $\sigma_{\bar{\alpha}}$. The final results are reported in Table 2 from where we see that the correction factor ranges between 0.4 and 0.7; i.e. the error is always within a factor of 2.[3]

[3]We have also applied the entire procedure by using the median to avoid the effect of outliers, but the final $\bar{\alpha}$ is not affected.

Table 2. Error propagation from averaging over the different simulations. The different columns refer to the different equations we are using for $D[H_3^+]$.

	(1)	(2)	(3)	(4)	(5)
$\bar{\alpha}$	0.7712	0.4528	0.4223	0.3881	0.5705
$\sigma_{\bar{\alpha}}$	0.0721	0.0414	0.0357	0.0308	0.0532

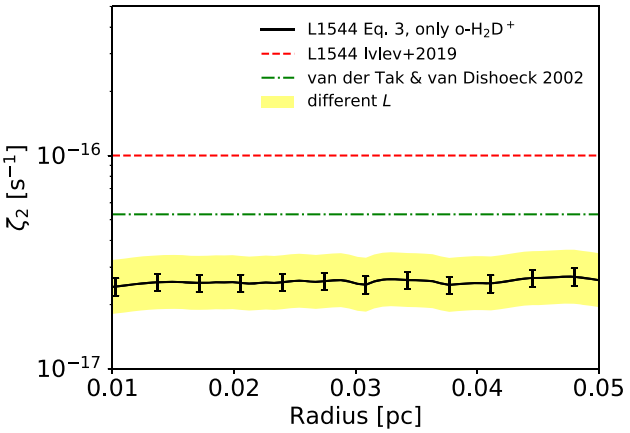

Figure 4. CRIR from equation (3), by employing the available column density profiles from Vastel et al. (2006). The green dot–dashed line is $\zeta_2 = 5.3 \times 10^{-17}$ s^{-1} reported by van der Tak & van Dishoeck (2000). The dashed red line instead represents the upper limit reported by Ivlev et al. (2019) for the same source. We have assumed a path-length of 0.034 pc, which is representative of the extension of *o*-H_2D^+ emission. The shaded area represents the variability of our results with *L*.

3.2 Application to L1544

To test our analytical approach, we have selected one of the best-studied low-mass cores, L1544, and used data from Vastel et al. (2006) who provide in their fig. 6 the radial profiles of the column densities for different tracers. With these data in hand, we computed the CRIR as shown in Fig. 4. We estimate the path-length by taking the geometrical average between the major and the minor axis of the *o*-H_2D^+ emission obtained by fitting the 50 per cent contour with an ellipse (see their fig. 4). We obtain $L = 0.034$ pc and $\zeta_2 \sim 2.5 \times 10^{-17}$ s^{-1}. However, we have to consider that the 3D shape of the core is not known; therefore, we also report the cases for *L* in between the major and the minor axis (yellow shaded area in Fig. 4). The CRIR moves to lower (higher) values with peaks around 3×10^{-17} s^{-1}. Overall, our estimated CRIR obtained from an unconstrained and a model-independent approach is close to typical values reported by van der Tak & van Dishoeck (2000),[4] but far from the value of $\zeta_2 \sim 10^{-16}$ s^{-1} measured in diffuse clouds and recently reported as upper limit by Ivlev et al. (2019) for the same pre-stellar core. Thus, chemistry appears to favour lower values of ζ_2 in dense cores.[5]

[4]We are using a CRIR per hydrogen molecule instead of per hydrogen atom as reported in the former paper, then there is a factor of 2.3 difference.
[5]To reach $\zeta_2 \sim 10^{-16}$ s^{-1}, *L* should be significantly smaller than the observed *o*-H_2D^+ emission towards L1544.

4 DISCUSSION AND CONCLUSIONS

In this letter, we propose and test an analytical approach to estimate the CRIR in the densest regions of molecular clouds. We have built the formula from first principles, under steady-state conditions, by following pioneering works in this field. The new idea behind the presented approach is based on two main components: (i) the estimate of the H_3^+ column density from its deuterated isotopologues and (ii) the validation of the methodology via 3D high-resolution simulations. This allowed us to explore different approximations and to test the statistical relevance of the approach by running an error analysis on different realizations. Overall, our method is providing small errors and a deviation from the real value of maximum a factor of 2. It is worth noting that the applicability of the formula depends on the availability of high-resolution observations being constrained by spatial scales (validity for $R \leq 0.05$ pc), in particular for CO that can be affected by freeze-out, and the H_3^+ isotopologues. In this respect, we propose different versions of the analytical formula to give more flexibility on its usage.

To further validate our results, we have applied the analytical formula to the well-studied low-mass core L1544, for which observations of the needed tracers exist, and we have found an average value for the CRIR of $2–3 \times 10^{-17}$ s^{-1}.

A very critical point of our approach is related to the path-length L. While theoretically we can provide a precise number for L, observationally this is an arbitrary choice. In McCall et al. (1999), L is obtained from a mix of observations and models as the ratio between the column and the number density of H_3^+. The column length can also be provided by the extension of the emission of the involved tracers, or by estimates of the size of the core. Considering the error analysis that we have performed on results that we can consider very robust, we can state that the main source of error in the presented approach comes from the choice of the path-length L.

To conclude, even considering the uncertainties coming from the choice of the path-length, and the intrinsic error that affects our approach, in particular the steady-state assumption, equation (3) represents the first attempt of providing a robust tool to evaluate the CRIR in dense cores, a parameter that has a strong impact on theoretical models, and on our understanding of star-forming regions.

ACKNOWLEDGEMENTS

SB was financially supported by CONICYT Fondecyt Iniciación (project 11170268). SB and DRGS were supported by CONICYT programa de Astronomia Fondo Quimal 2017 QUIMAL170001. AL acknowledges support by the European Research Council No. 740120 'INTERSTELLAR'. SF-C was supported by CONICYT Programa de Astronomía Fondo ALMA-CONICYT 2017 Project #31170002. We are grateful to Alexei Ivlev for useful discussions on the draft.

REFERENCES

Bialy S., 2020, Commun. Phys., 3, 32
Black J. H., Hartquist T. W., Dalgarno A., 1978, ApJ, 224, 448
Bovino S., Ferrada-Chamorro S., Lupi A., Sabatini G., Giannetti A., Schleicher D. R. G., 2019, ApJ, 887, 224
Brünken S. et al., 2014, Nature, 516, 219
Caselli P., 2002, Planet. Space Sci., 50, 1133
Caselli P., Walmsley C. M., Terzieva R., Herbst E., 1998, ApJ, 499, 234
Caselli P., Walmsley C. M., Tafalla M., Dore L., Myers P. C., 1999, ApJ, 523, L165
Caselli P., van der Tak F. F. S., Ceccarelli C., Bacmann A., 2003, A&A, 403, L37
Caselli P., Vastel C., Ceccarelli C., van der Tak F. F. S., Crapsi A., Bacmann A., 2008, A&A, 492, 703
Ceccarelli C., Dominik C., Lefloch B., Caselli P., Caux E., 2004, ApJ, 607, L51
Ceccarelli C., Caselli P., Bockelée-Morvan D., Mousis O., Pizzarello S., Robert F., Semenov D., 2014, in Beuther H., Klessen R. S., Dullemond C. P., Henning T., eds, Protostars and Planets VI. University of Arizona Press, Tucson, AZ, p. 859
Dalgarno A., 2006, Proc. Natl Acad. Sci. USA, 103, 12269
Fontani F. et al., 2011, A&A, 529, L7
Fontani F., Giannetti A., Beltrán M. T., Dodson R., Rioja M., Brand J., Caselli P., Cesaroni R., 2012, MNRAS, 423, 2342
Geballe T. R., Oka T., 1996, Nature, 384, 334
Giannetti A. et al., 2014, A&A, 570, A65
Giannetti A. et al., 2019, A&A, 621, L7
Hopkins P. F., 2015, MNRAS, 450, 53
Indriolo N., 2012, Phil. Trans. R. Soc. A, 370, 5142
Ivlev A. V., Silsbee K., Sipilä O., Caselli P., 2019, ApJ, 884, 176
Kong S., Caselli P., Tan J. C., Wakelam V., Sipilä O., 2015, ApJ, 804, 98
Körtgen B., Bovino S., Schleicher D. R. G., Stutz A., Banerjee R., Giannetti A., Leurini S., 2018, MNRAS, 478, 95
McCall B. J., Geballe T. R., Hinkle K. H., Oka T., 1999, ApJ, 522, 338
Neufeld D. A., Wolfire M. G., 2017, ApJ, 845, 163
Oka T., 2019, Phil. Trans. R. Soc. A, 377, 20180402
Pagani L., Salez M., Wannier P. G., 1992, A&A, 258, 479
Sabatini G., Giannetti A., Bovino S., Brand J., Leurini S., Schisano E., Pillai T., Menten K. M., 2019, MNRAS, 490, 4489
Shingledecker C. N., Bergner J. B., Le Gal R., Öberg K. I., Hincelin U., Herbst E., 2016, ApJ, 830, 151
van der Tak F. F. S., van Dishoeck E. F., 2000, A&A, 358, L79
Vastel C., Caselli P., Ceccarelli C., Phillips T., Wiedner M. C., Peng R., Houde M., Dominik C., 2006, ApJ, 645, 1198
Vaupré S., Hily-Blant P., Ceccarelli C., Dubus G., Gabici S., Montmerle T., 2014, A&A, 568, A50

This paper has been typeset from a TEX/LATEX file prepared by the author.